**EPJ manuscript No.**
(will be inserted by the editor)

# Self-assembly of smart mesoscopic objects

J.Metzmacher, M.Poty, G.Lumay, and N.Vandewalle

GRASP, CESAM Research Unit, Institute of Physics B5a, University of Liège, B4000 Liège, Belgium.

the date of receipt and acceptance should be inserted later

**Abstract.** Self-assembly due to capillary forces is a common method for generating 2D mesoscale structures made of identical particles floating at some liquid-air interface. We show herein how to create soft entities that deform or not the liquid interface as a function of the strength of some applied magnetic field. These smart floating objects self-assemble or not depending on the application of an external field. Moreover, we show that the self-assembling process can be reversed opening ways to rearrange structures.

## 1 Introduction

Self-assembly offers opportunities for elaborating mesoscale structures between bottom-up and top-down fabrication methods [1,2]. In particular, capillary driven self-assembly is a physical process in which small components form spontaneously an ordered structure along a liquid surface. Although numerous examples of capillary driven self-assembly have been given in the literature [3,4], the creation of complex structures or functional systems is still a challenge [5].

When a few particles are placed on a liquid surface, the local deformation of the interface around each particle induces capillary interactions driving the system into random structures in most cases [6,7]. A few models have been proposed to describe the capillary interaction of particles [8–10]. Vella and Mahadevan [11] rationalized this interaction for spherical particles only. Other approaches [12,13] were proposed for non-spherical particles and complex objects. The cylindrical liquid profile, being the liquid elevation $z_i$, around a spherical particle, labelled $i$, is given by

$$z_i = Q_i K_0\left(\frac{r}{\lambda}\right) \tag{1}$$

where $Q_i$ is called a capillary charge and corresponds roughly to a characteristic depth for the liquid deformation around the particle. The function $K_0(x)$ is the modified Bessel function of the second kind. The typical distance $\lambda = \sqrt{\gamma/\rho g}$, over which the liquid surface is deformed, is called the capillary length, which depends on surface tension $\gamma$ and liquid density $\rho$. This characteristic length is close to $\lambda = 2.7\,\mathrm{mm}$ for water. The scale $\lambda$ gives the range of lengths corresponding to the mesoscopic world for capillary systems. In Eq. (1), the distance $r$ is counted from the object center. When two distant particles, labelled $i$ and $j$, are floating at the liquid surface, the interaction potential is given by

$$U_{ij} = -2\pi\gamma Q_i Q_j K_0\left(\frac{r_{ij}}{\lambda}\right) \tag{2}$$

where the product of the capillary charges is found. This potential results from the superposition of the deformations $z_i$ and $z_j$, which is assumed even if observations show that the superposition principle is a crude approximation [14]. Both attraction and repulsion can be obtained, depending on the respective signs of the capillary charges $Q_i$ and $Q_j$. For distant objects ($r_{ij}/\lambda \gg 1$), the decay of $K_0$ looks like an exponential decay such that the interaction is driven by short range effects.

Some attempts have been made to control the capillary assembly by the use of an external field [15]. For example, Singh et al. [16] applied an electric field to eliminate the defects and control the spacing of monolayers. The curvature of the interface can also be employed to modify the assembly [12].

When the particle shape differs from a sphere, or when the contact line oscillates along the particle sides, capillary multipole, *i.e.* the superposition of both positive and negative capillary charges, has been proposed for describing the deformation of the liquid around some anisotropic particles [17,18]. These capillary multipoles were the key ingredients of our earlier works [19]. Indeed, we created cross-shaped objects with specific curvatures in order to induce local liquid deformations at the branch tips. Each tip is therefore characterized by a specific capillary charge. Using this method, we were able to program self-assembled structures with desired symmetries such as square and triangular lattices [19]. In the same study, we also demonstrated that complex arrangements with fivefold symmetries can be obtained.

In this paper, we propose to increase our knowledge about these capillary multipolar interactions by fabricating smart objects, *i.e.* floating entities that are able to change their interactions by the application of an external field. Our results will also contribute to the fabrication of active components for capillary driven self-assembly.

## 2 Methods

We created cross-shaped entities by polymer molding. We use liquid vinylpolysiloxane. The Young modulus of this polymer is low ($Y \approx 1\,\mathrm{MPa}$) allowing for relevant elastic deformations [20]. The cross-shaped objects, as illustrated in Fig. 1, have a hole in their center, in order to favor significant deformations of the four branches. The branch length is $L = 10\,\mathrm{mm}$ and the branch width is $\ell = 4\,\mathrm{mm}$. Near the center, a neodym magnet (1 mm thick) is inserted in each branch.

When a vertical magnetic field is applied through the system, the magnetic dipoles tend to orient themselves to the field orientation. This induces a deformation of the branches, as illustrated in Figs. 1(a) and 1(b) where the effect of respective downward and upward fields are shown on the same object. The magnetic field is generated by Helmholtz coils. As the object floats in the center of the coils, we can consider that the field is nearly uniform. It should be noted that capillary charges are expected to appear at the extremities of the branches. So, considering these charges are created by spherical particles, the leading dimension of the system is the branch width, which is of the order of the capillary length $\lambda$. Considering the capillary scale, our system belongs therefore to the mesoscale.

It should be remarked that depending on the orientation of the dipoles in the branches, a magnetic field can create either positive or negative capillary charges. This is of high interest in order to control repulsion / attraction between identical floating entities. For our study, we decided to work with a single configuration with all dipoles pointing on the center, as sketched in Fig. 1. Following our previous works on capillary multipoles [19], we expect that objects with similar capillary charges on all tips will induce a square lattice. In fact, different configurations are possible with a part of the magnets having a different orientation than others. A magnetic coding of the branches is possible but left for future works.

Due to the molding process, all the parts of the entities are not in contact with the same material when the vinylpolysiloxane cures. The contact angles of the different parts of the cross-shaped objects were measured with a contact anglemeter CAM 200 from KSV Ltd. All the parts of the entities are hydrophobic : the side and the lower faces, in contact with the polymer of the mold, have a contact angle $\theta_l = 133 \pm 1°$ and the upper face, in contact with air, has a contact angle $\theta_u = 98 \pm 1°$. So, our objects are partially wetted. We create sharp edges between the side and the upper faces (see Fig. 1). Our objects being denser than water, the meniscus is therefore pinned on these sharp edges [21]. Pinning means that contact angle is no more a key property of our objects.

In order to study the self-assembled patterns, we used large Petri dishes, or even large containers, filled with pure water. The liquid-air interface is placed in a coil producing a uniform magnetic field, ranging from 0 G to 55 G. A camera takes pictures from above. For characterizing our multipoles, we used an optical method proposed by Moisy et al. [22] for imaging the small deformations of a liquid-air interface around a single floating body. The method is based on light refraction. A random pattern is placed at the bottom of the container, the camera records pictures of that pattern through a flat interface, *i.e.* without any object. After placing the object at the interface, new pictures of the pattern are taken. Series of pictures, with and without objects, are compared. Then, image correlations are used to reconstruct the 3d shape of the interface.

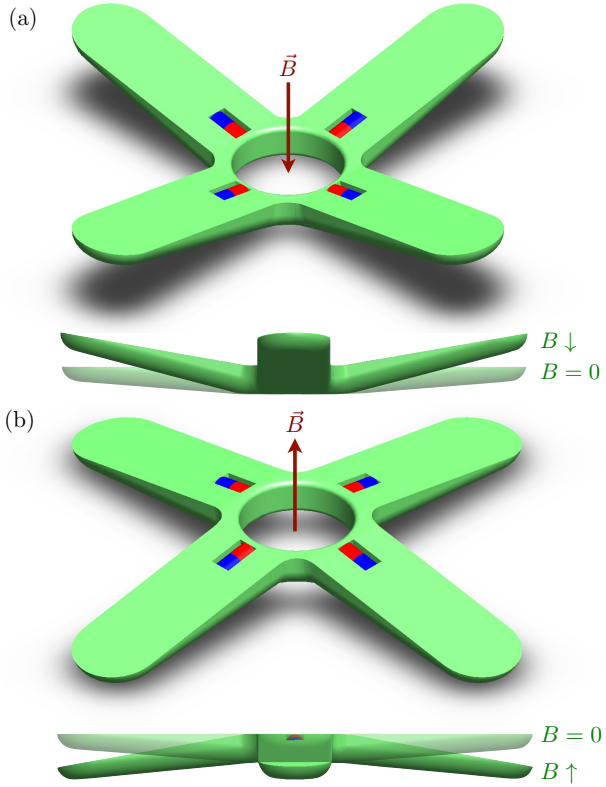


**Fig. 1.** Close view and side view of the cross-shaped soft object we consider in this paper. All magnets are oriented towards the center of the object. (a) When submitted to a vertical downward field, the dipoles inserted in the branches induce a positive deformation. (b) When the field is reversed, the dipoles induce a negative deformation of the branches.

Finally, it should be noted that the permanent magnets are located near the center of the floating bodies such that the interaction between dipoles coming from neighboring entities is weak but non zero. This effect will be discussed in sect. 3.2.

## 3 Results

### 3.1 Smart entities

We characterized the liquid deformations around each basic elements using the Moisy profilometry technique [22]. Experimental liquid profiles around the particles are shown in the color scale of Fig. 2 : red for positive deformation and blue for negative deformation. Two cases are shown :

(a) $B = 0$ and (b) $B \neq 0$ downward. In Fig. 2(a), one expects a flat object with a limited deformation of the liquid surface. Nevertheless, one observes a negative deformation around the center of the object, being the consequence of the own weight of the object. Weak positive deformations can also appear near branch tips, due to the natural deformation of the object on the liquid surface. This nonzero deformation at $B = 0$ will be measured below.

In Fig. 2(b), the magnetic field is switched on and strong deformations are observed near branch tips, as expected. The negative capillary charge observed in the center of the element seems also strengthened.

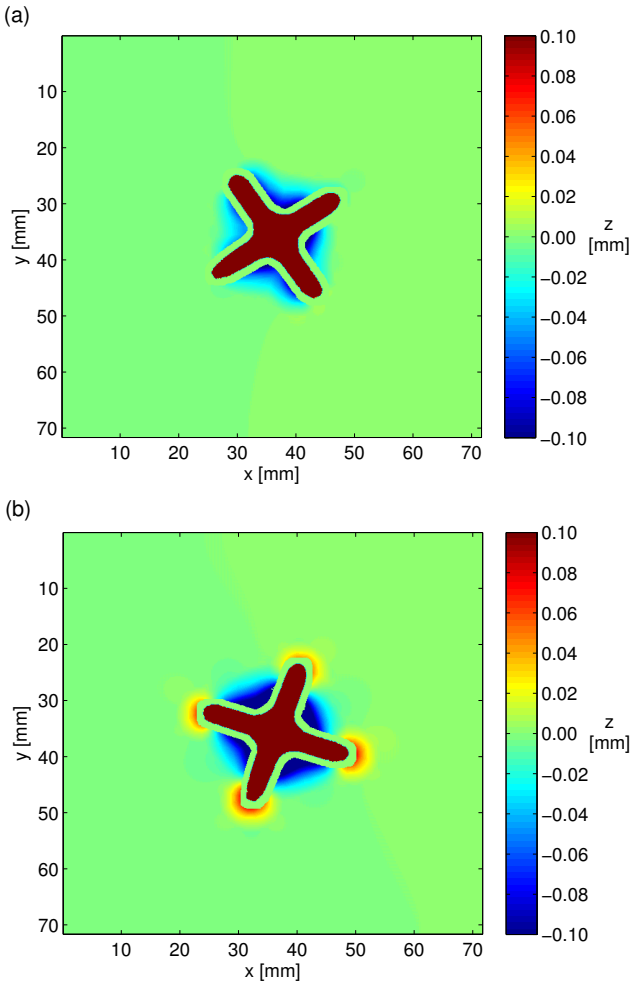


**Fig. 2.** Profile $z(x, y)$ of the liquid surface around the objects in a color scale, as measured by the Moisy method. (a) Free floating crossed object with $B = 0$. The natural deformation creates a negative (blue) charge near the center and weak positive charges at the branch tips. (b) When the magnetic field is switched on ($B = 41\,\mathrm{G}$), the positive capillary charges are well pronounced at branch tips. Capillary interactions between similar objects are expected to be more important in this case than in (a).

In order to characterize the capillary charges created by our smart objects, we use as a model a linear combination of charges : a central pole $Q_c$ located at the center of the object and 4 identical dipoles placed along the branches. The dipoles correspond to a charge $-Q_{br}$ at the center of the object and an opposite charge $+Q_{br}$ located at the tip of the branch. Indeed, when we lift an arm the tip creates a positive capillary charge whereas the other extremity creates a negative charge. The data from Fig. 2 are fitted by this model of Eq. (1) with only two free fitting parameters, $Q_c$ and $Q_{br}$. The resulting liquid profiles are shown in Fig. 3. We can observe that our model is in good agreement with our experimental data, especially when the magnetic field is applied.

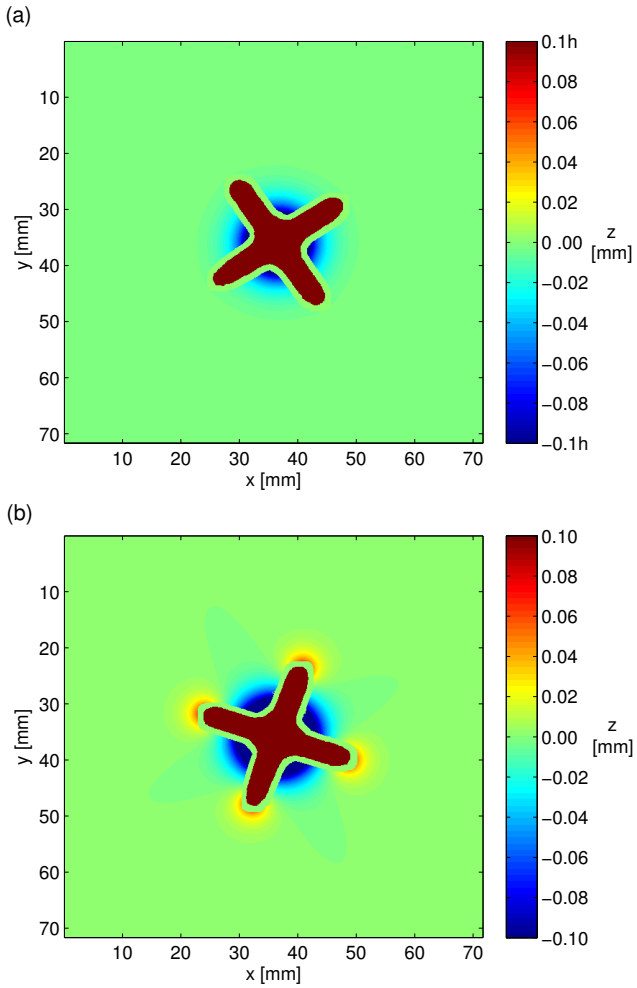


**Fig. 3.** Profile $z(x, y)$ of the liquid surface around the same object of Fig. 2, as fitted using Eq. (1) and a linear combination of a central pole and 4 identical dipoles. The profiles should be compared to the ones of Fig. 2. (a) Free floating crossed object with $B = 0$. (b) Free floating crossed object when the magnetic field is switched on ($B = 41\,\mathrm{G}$).

The capillary charges $Q_{br}$ of the dipoles are then extracted from the model and shown as a function of $B$ in

Fig. 4. The capillary charge increases linearly with the applied field strength. This can be understood from the following arguments. By defining the angle $\theta$ between each branch (each dipole) and the horizontal plane, one has a dimensionless deformation $\varepsilon = \sin\theta$ and a capillary charge given by $Q_{br} = L\sin\theta$. Considering the competition between both magnetic and elastic energies for each branch, one has some energy per unit volume given by

$$u = -\mu B\varepsilon + \frac{1}{2}Y\left(\varepsilon - \varepsilon_0\right)^2 \qquad (3)$$

where $Y$ is the Young modulus, $\mu$ being the dipole moment per unit volume, and $\epsilon_0$ the natural deformation on the liquid surface for $B = 0$, as evidenced in Fig. 2(a). The equilibrium situation, given by $\frac{\partial u}{\partial \varepsilon} = 0$, is found, and the resulting capillary charge is

$$Q_{br} = Q_{br,0} + \frac{\mu BL}{Y} \qquad (4)$$

where $Q_{br,0} = L\varepsilon_0$ is the natural capillary charge. The above physical ingredients predict a linear behavior for the capillary charge as a function of $B$. The fit is given in Fig. 4, in excellent agreement with our data. When the field is zero, the natural capillary charge on branches $Q_{br,0}$ remains weak, around 0.003 mm. The ratio $\mu B/Y$ should be considered as a magnetoelastic number which characterizes the ability to deform under a magnetic field. From the above results, we can conclude that we created soft objects responding significantly to an external field.

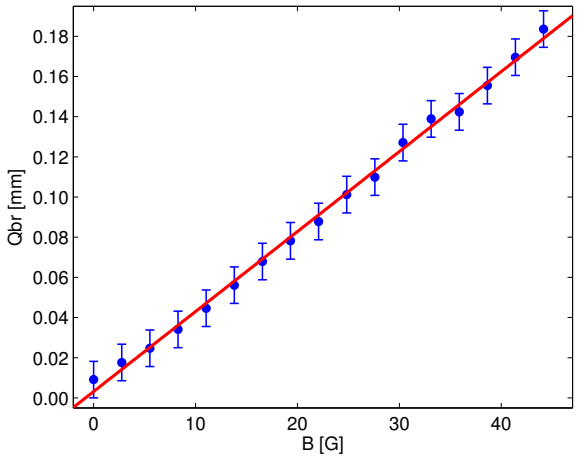


**Fig. 4.** The capillary charge $Q_{br}$ on each dipole as a function of $B$. A linear trend intercepts the vertical axis determining a weak natural capillary charge $Q_{br,0} \approx 0.003\,\mathrm{mm}$, close to zero.

We can also extract from the data the change of the central pole as a function of $B$ (see Fig. 5). Like the dipoles the central capillary charge is evolving linearly with the applied field strength. This can be understood from the following arguments. When the magnetic field is applied, the dipoles do not only rotate. They also exert a vertical force proportional to $B$ that pushes the object down until the vertical component of surface tension counterbalances it. It increases the depth of the liquid deformation, in particular around the center of the object. So, it strengthens the capillary charge $Q_c$.

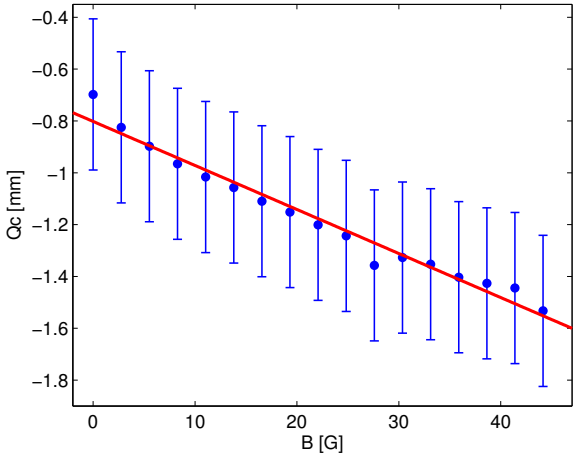


**Fig. 5.** The capillary charge $Q_c$ of the central pole as a function of $B$. A linear trend intercepts the vertical axis determining the natural capillary charge $Q_{c,0} \approx -0.8$ mm.

### 3.2 Self-assemblies

Let us now consider a few smart entities in a large container in order to avoid as much as possible the capillary interactions with the borders. Self-assembly takes place in the center of the container, where the magnetic field can be considered as nearly uniform.

Figures 6(a-f) present top pictures of Petri dishes in which freely floating entities are in interaction. In the first picture (a), the entities are interacting without the presence of an external field. The entities are flat and only weak deformations of the liquid-air interface are expected. The weak capillary interactions are in fact completely dominated by the magnetic repulsive interactions between neighboring entities. As a result, the floating objects remain separated from each other. They possess particular relative orientations. Because of the dipole-dipole repulsive interactions, two neighboring objects separated by some distance tend to rotate by 45° from each other. This effect can be well observed in Fig. 6(a).

In Fig. 6(b), a vertical magnetic field is applied through the system, starting from the situation (a). The local deformations induce positive capillary charges at each tip such that the capillary interactions become more and more important as the field increases. A square pattern emerges when capillary interactions dominate magnetic repulsion. The self-assembly into a crystal-like structure can therefore be induced by the external field.

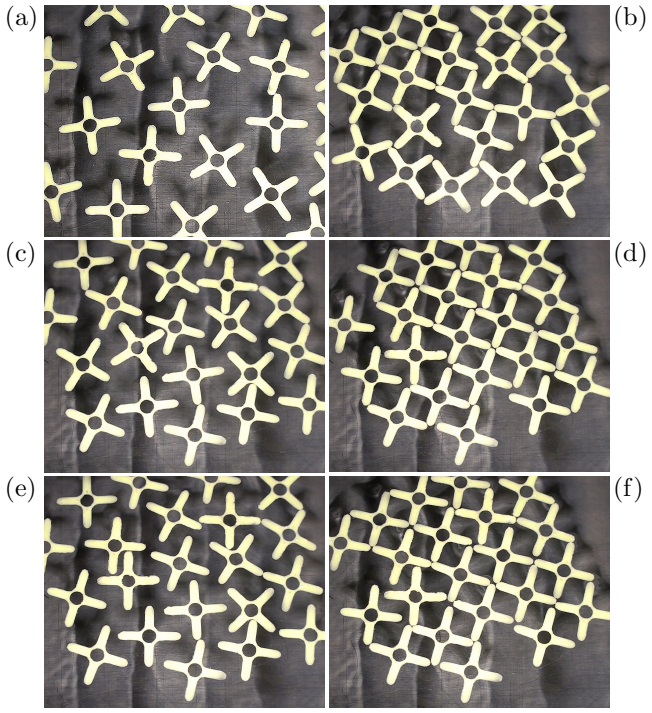


**Fig. 6.** Images of the center of the container where a few entities are freely floating with or without a magnetic field. The series of pictures (a) to (f) corresponds to alternating sequences during which the field is on/off. Left column: magnetic field off; right column: magnetic field on.

### 3.3 Annealing

When the structure is created with a strong magnetic field, one observes the formation of an imperfect crystal with defects such as vacancies and grain boundaries, as seen in Fig. 6(b). The ordering of the floating particles is incomplete but they stick together. By decreasing or suppressing the external field, one expects that the magnetic entities inserted in the objects dominate the capillary forces such as particles detach from each other, keeping nearly similar positions and orientations.

The melting of the self-assembly is indeed observed in Fig. 6(c) when the field of Fig. 6(b) is switched off. The capillary driven self-assembling process is therefore reversible. This allows a slow reorientation of the particles. A second self-assembly, when the field is switched on, is showing a better arrangement. See Fig. 6(d). Less defects are seen in the square pattern.

Annealing cycles can be considered to decrease the fraction of defects in the target structure. Figures 6(e-f) show a third cycle, improving again the structure. This should depend on parameters such as (i) timescales for vanishing/increasing magnetic fields, (ii) strength of the magnetic fields and (iii) cycle numbers. It is of interest to study the way structures can be improved by annealing but this remains outside the scope of the present paper.

## 4 Summary

We created smart entities for capillary driven self-assembling along a liquid interface. By smart we mean entities that are able to modify their interaction from the application of an external field. We show that magnetic inclusions in elastic objects are able to deform the entities. The process is reversible allowing to both aggregation and separation processes. We show that annealing can be considered to improve the quality of resulting self-assemblies thanks to the reversible character of the processes.

It should be remarked that such material can be used to any small elastic object. By small, we consider that the gravity effect should be dominated by magnetoelastic effects. Magnetic remanence could be also used to induce a memory of the intial shape [23]. Many applications can be found in microfabrication as well as in self-assembled robotics. Indeed, oscillating fields may induce locomotion as recently demonstrated in [23–26].

## Acknowledgments

This work is financially supported by the University of Liège and CESAM Research Unit.

## Author contribution statement

JM and MP carried out the experiments and performed the data treatments. All the authors contributed to the writing of the manuscript.

## References

1. G.M.Whitesides and B.Grzybowski, Science **295**, 2418 (2002)
2. J.A.Pelesko, *Self-Assembly*, (Chapmann & Hall, Boca Raton, 2007)
3. R.R.A.Syms, E.M.Yeatman, V.M.Bright, G.Whitesides, J. Microelectromech. Sys. **12**, 387 (2003)
4. A.Demortière, A.Snezhko, M.V.Sapozhnikov, N.Becker, T.Proslier, I.S.Aranson, Nature Comm. **5**, 3117 (2014)
5. M.Boncheva and G.M.Whitesides, MRS Bull. **30**, 736 (2005)
6. M.Berhanu and A.Kudrolli, Phys. Rev. Lett. **105**, 098002 (2010)
7. M.J.Dalbe, D.Cosic, M.Berhanu and A.Kudrolli, Phys. Rev. E **83**, 051403 (2011)
8. P.A.Kralchevsky and K.Nagayama, J. Colloid Interface Sci. **85**, 145 (2000)
9. M.Oettel and S.Dietrich, Langmuir **24**, 1425 (2008)
10. A. Dominguez, *Structure and functional properties of colloidal systems*, (CRC Press, Boca Raton, 2010) p.31
11. D.Vella and L.Mahadevan, Am. J. Phys. **73**, 817 (2005)
12. L.Botto, E.P.Lewandowski, M.Cavallaro, Jr. and K.J.Stebe, Soft Matter **8**, 9957 (2012)
13. P.A.Kralchevsky and N.D.Denkov, Curr. Opin. Colloid **6**, 383 (2001)
14. M.Nicolson, Proc. Cambr. Phil. Soc. **45**, 288 (1949)

15. N.Vandewalle, N.Obara and G. Lumay, Eur. Phys. J. E **36**, 127 (2013)
16. P.Singh, D.D.Joseph and N.Aubry, Soft Matter **6**, 4310 (2010)
17. J.C.Loudet, A.G.Yodh and B.Pouligny, Phys. Rev. Lett. **97**, 018304 (2006)
18. G.B.Davies, T.Kruger, P.V.Coveney, J.Harting, and F.Bresme, Adv. Mater. 26, 6715 (2014)
19. M.Poty, G.Lumay and N.Vandewalle, New J. Phys. **6**, 023013 (2014)
20. N.Adami and H.Caps, EPL **106**, 46001 (2014)
21. W.-J.A.de Wijs, J.Laven and G.de With, AIChE J. **62**, 4453 (2016)
22. F.Moisy, M.Rabaud and K.Salsac, Exp. Fluids **46**, 1021 (2009)
23. E.Diller, N.Zhang, M.Sitti, J. Micro-Bio Robot **8**, 121 (2013)
24. A.Snezhko and I.S.Aranson, Nature Mat. **10**, 698 (2011)
25. G.Lumay, N.Obara, F.Weyer, N.Vandewalle, Soft Matter **9**, 2420 (2013)
26. G.Grosjean, G.Lagubeau, A.Darras, M.Hubert, G.Lumay and N.Vandewalle, Sci. Reports **5**, 16035 (2015)